DFT design of polyguanidine – a unique two-dimensional material with high-energy density

Sergey V. Bondarchuk & Boris F. Minaev

➕ View supplementary material ↗

📅 Published online: 08 May 2017.

✎ Submit your article to this journal ↗

📊 Article views: 20

🔍 View related articles ↗

◑ View Crossmark data ↗

❐ Citing articles: 1 View citing articles ↗

Taylor & Francis
Taylor & Francis Group

RESEARCH ARTICLE

Check for updates

DFT design of polyguanidine – a unique two-dimensional material with high-energy density

Sergey V. Bondarchuk [a] and Boris F. Minaev[a,b]

[a]Department of Chemistry and Nanomaterials Science, Bogdan Khmelnitsky Cherkasy National University, Cherkasy, Ukraine; [b]Division of Theoretical Chemistry and Biology, School of Biotechnology, KTH Royal Institute of Technology, Stockholm, Sweden

ABSTRACT

We report herein a theoretical prediction and characterisation of a new two-dimensional (2D) material based on energetic polyguanidine. The structure represents a hexagonal type lattice of the *P6/m* space group. The material is dynamically and mechanically stable. Highly accurate band structure calculation with hybrid functional HSE06 reveals a tiny direct band gap being equal to 0.181 eV. We provide an additional spectral characterisation of the 2D polyguanidine substance including UV-vis, nuclear magnetic resonance and nuclear quadrupolar resonance parameters. The electron transport properties of a 26.6 Å wide polyguanidine ribbon are calculated in terms of tight-binding density functional theory approach. The predicted 2D material is also analysed by means of Quantum Theory of Atoms in Molecules and the aromatic character of the formed rings is estimated using nucleus-independent chemical shifts quantities.

1. Introduction

Two-dimensional (2D) materials with high nitrogen content demonstrate a sustainable growing interest due to their interesting electronic and thermochemical properties [1,2]. Usually obtained by an exfoliation of the corresponding layered bulk materials [3], the 2D structures possess quite different properties due to the high surface-bulk ratio and the absence of the interlayer interaction [4,5]. Though the discovery of the first 2D material, graphene, was first reported in 2004 by Novoselov *et al.* [6], the synthesis of 2D materials other than graphene still remains to be rare. Graphene itself demonstrated a limited application due to a lack of intrinsic band gap [7].

Meanwhile, guanidine has a high nitrogen content (71.1 wt %), and in the protonated form, it is often considered as an energetic ion in the high-energy density materials [8]. Guanidine forms salts via a proton transfer from another energetic molecules, usually from the neighbour OH-groups of different bis(1H-tetrazole) derivatives [9]. Besides these molecular counterparts, guanidine forms salts with different other energetic compounds, and among those one can find dinitromethanides, which are characterised by a low impact sensitivity (>40 J) [10];

⊕ Supplemental data for this article can be accessed at ⊘ http://dx.doi.org/10.1080/00268976.2017.1321157.
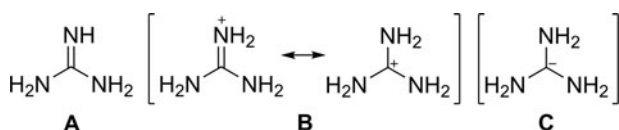
Scheme 1. Neutral and ionic forms of guanidine.

for example, 5-nitroguanidyltetrazole [11], nitroformate [12], 1-amino-1-hydrazino-2,2-dinitroethene [13], 3,3′-dinitro-5,5′-azo-1,2,4-triazolate [14], 5,5′-azotetrazolate [15] and bis[4-nitraminofurazanyl-3-azoxy]azofurazan [16]. In acidic solution, guanidine can condensate with alcohols and aldehydes [17,18], which may be a potential route to the 2D polymer preparation.

Guanidine also includes numerous applications in biological systems. When bonded with phosphate residue, guanidinium moiety enhances peptide transport through liposomal and cell membranes [19]. This moiety is one of the building blocks of batzelladines, a family of highly complex polyguanidinium alkaloids, which were isolated from the Caribbean sponge Batzella sp. [20]. Recently developed guanidinium ionic liquids exhibit remarkable chemical properties, which are applied for separation of multiple types of glycoproteins [21] or selective enrichment of phosphopeptides [22]. Apart from the biological applications, the guanidine is used as an additive to dye-sensitised solar cells in order to improve their performance [23] as well as to hybrid perovskite solar cells to enhance carrier lifetime and open-circuit voltage [24]. To form water insoluble low-toxic disinfectants or biocides, guanidine is coated on thin-film composite polymers as well [25].

As we have mentioned above, guanidine (Scheme 1(A)) can be easily protonated to form an onium (guanidinium) cation (B); the latter has two main resonance contributions with the N and C-atoms being positively charged (Scheme 1). The guanidinium cation remains protonated over a much wider range of pH than does the ammonium group [26].

Due to the presence of a $2p_\pi$ orbital at the sp^2-hybridised carbon atom, guanidine can acquire one or two electrons forming the corresponding radical and anion (Scheme 1(C)). Thus, it becomes clear that the asymmetric cell of the 2D polyguanidine should combine two guanidine moieties B and C. From this point of view, it is interesting to model and study a 2D material based on the guanidine molecule, which has been performed in the presented work.

2. Computational details

Periodic density functional theory (DFT) calculations have been performed using Cambridge Serial Total Energy Package code [27] as implemented in Materials Studio 7.0 suite of programs [28]. All the calculations presented in this work have been performed at two levels of theory, namely, local density (LDA) and generalised gradient (GGA) approximation. Within the GGA approach, cell relaxation, nuclear magnetic (NMR) and quadrupolar (NQR) resonance properties as well as the electron transport characteristics have been calculated using the functional parameterised by Perdew–Burke–Ernzerhof (PBE) [29]. Mechanic properties have been obtained by using the modified functional, namely, PBE for solids [30]. Finally, the band structure and optical properties calculations have been carried out using a highly accurate hybrid functional by Heyd–Scuseria–Ernzerhof (HSE06) [31]. The latter functional has been recently proven to produce the band gaps being close to ones experimentally obtained results [32]. For GGA/PBE approach, the long-range correlations have been taken into account entirely using the Tkatchenko–Scheffler (TS) scheme [33]. Within the LDA approach, we have applied the functional due to Ceperley and Alder [34] as parametrised by Perdew and Zunger [35], namely, CA-PZ. The long-range correlations were taken into account using scheme by Ortmann–Bechsted-Schmidt [36].

Description of the electron–core interactions has been presented entirely using the norm-conserving pseudopotentials (NCPs). In the case of phonon dispersion calculations, which have been performed with the finite displacement method, the Vanderbilt type pseudopotentials have been applied. Such approach was recently proven to be reliable [37,38]. Finally, for the Quantum Theory of Atoms in Molecules (QTAIM) analysis, the wave functions have been obtained using the projector augmented wave based method [39] as part of the Quantum Espresso 4.3.2 program package [40]. The QTAIM analysis has been carried out using the CRITIC2 software [41].

During calculations, the electronic wave functions have been expanded in a plane wave basis set with an energy cut-off of 1000 eV (73.5 Ry). The Monkhorst–Pack k-point sampling scheme with a $6 \times 6 \times 2$ (0.03 1/Å) k-point mesh has been specified entirely except of band structure calculations. For this case, a looser mesh of $3 \times 3 \times 2$ (0.06 1/Å) and 700 eV (51.4 Ry) energy cut-off has been utilised since this provides minimal settings for reproducing stable results [42]. To avoid unphysical interactions between the layers, a 15 Å vacuum slab has been added at the starting point. Thereafter, the complete cell relaxation has been allowed.

Finally, the molecular DFT calculations have been performed using the GAUSSIAN09 suite of programs [43]. The wave functions have been obtained by the B3LYP method [44] with the Pople's split-valence quasi triple-ζ basis set
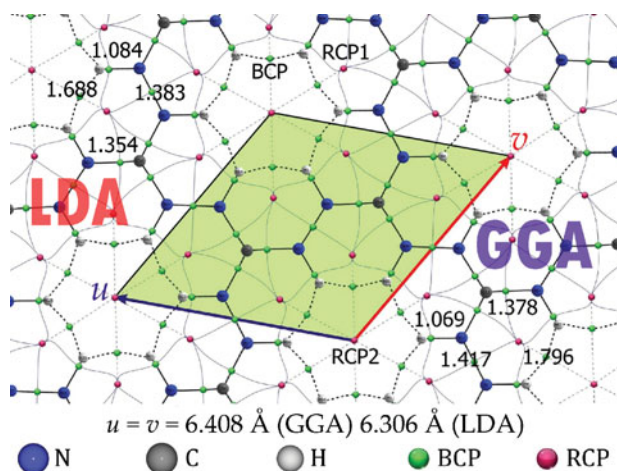
Figure 1. The optimised asymmetric cell and the topological parameters of the 2D polyguanidine (bond lengths are in Å).

(6-311 G) and addition of both the polarisation (d, p) and diffuse (+) functions [45].

3. Results and discussion

3.1. Structure and electronic properties

The optimised asymmetric cell of the 2D polyguanidine along with the bond critical points (BCP), paths and ring critical points (RCP) is illustrated in Figure 1 and the packing of the layer is presented in Figure S1 in the Supporting Information. Geometry optimisation has led to the hexagonal lattice of the $P6/m$ space group (the Laue class $6/m$) for the supercell. All the atoms occupy the Wyckoff position 6j: C (0.333, 0.667, 0), N (0.383, 0.900, 0) and H (0.240, 0.937, 0). As it follows from Figure 1, there are three non-equivalent bond lengths. The N–N bond length is equal to 1.417 Å, which is slightly less than in the recently predicted trigonal nitrogen allotrope (1.436 Å) [42]. The N–H bonds are significantly elongated (1.069 Å) which can be attributed with a strong NH-acidity. Similar results are obtained at the LDA level of theory, but the structural parameters are bit smaller (Figure 1). According to the Hirshfeld population analysis, the carbon atoms are slightly positively charged (+0.16) and the nitrogen atoms are negatively charged (−0.08). Thus, a strong charge delocalisation occurs which tends to equalisation of all the bond lengths within the cell. The 2D polyguanidine has a strong cohesive energy, which has been calculated using Equation (1). The obtained value is 7.07 eV/atom (6.55 eV/atom at the LDA level of theory) indicating a good robustness of the studied solid.

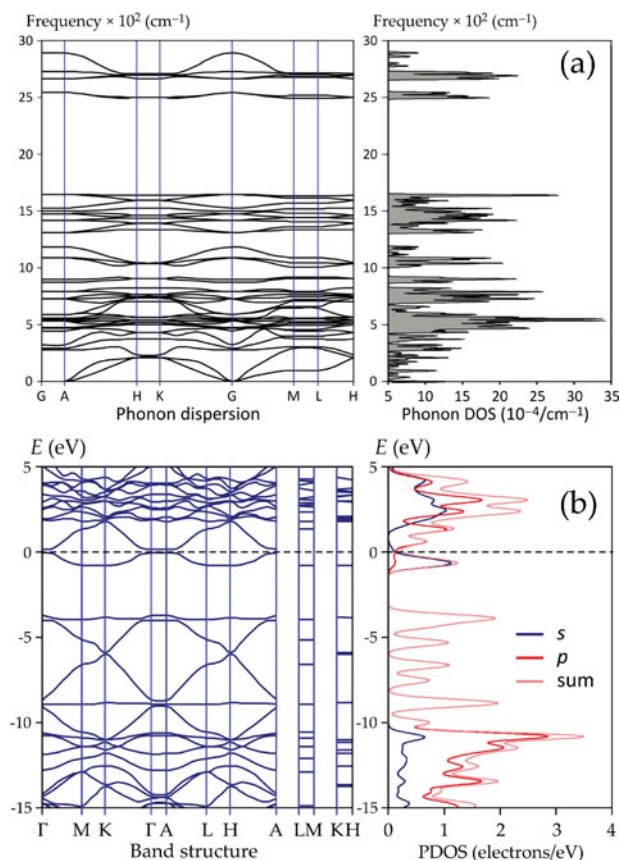$$E_{coh} = -(1/2E_{phase} - (E_C + 3E_N + 3E_H))/7, \quad (1)$$

Figure 2. Phonon dispersion and density of phonon states (a) as well as band structure and partial density of states (PDOS) (b) for the 2D polyguanidine.

where E_{phase} is the total enthalpy (PBE-TS) of the 2D polyguanidine; E_C, E_N and E_H are the total enthalpies of an isolated carbon, nitrogen and hydrogen atom, respectively; these have been obtained in terms of the supercell approximation (vacuum slab thickness is 15 Å).

In order to estimate the dynamical stability of the 2D polyguanidine, we have performed phonon dispersion calculation. The obtained results along with the phonon density of states at the GGA/PBE level of theory are illustrated in Figure 2(a). A similar result was obtained using the LDA approach. The phonon spectrum has total 42 modes, from which 39 modes are optical. As one can see in Figure 2(a), the obtained spectrum for 2D polyguanidine is characterised by the absence of soft modes. At the $q = 0$ the N–H valence vibration equals to 2893 cm^{-1} being significantly lower than the usual frequencies of this type vibrations (>3000 cm^{-1}). This suggests a specific form of very weak N–H bonds. With the rise of q-vector, this branch decreases sharply which can be attributed to the preferable out-of-plane position of the N–H bonds. Probably, another non-planar phase of the C$_{3v}$ point group should exist. The symmetry reduction down to the trigonal crystal system can produce

other stable polymorphs; therefore, this requires further more detailed study.

An interesting question about the band structure of 2D polyguanidine material arises after vibrational analysis. To answer this question, we have performed two calculations of the band structure in terms of the high-throughput approximation, which includes a standard definition of the high symmetry k-path for all the 14 Bravais lattices [46]. For the hexagonal lattice, the Brillouin zone integration scheme along with the corresponding k-path is illustrated in Figure S2 and the definition of k-points is presented in Table S1 in the Supporting Information.

We have applied a highly accurate approach NCP/HSE06/700 eV and the results are graphically illustrated in Figure 2(b). As it follows from the band structure plot, the 2D polyguanidine sheet possesses a tiny direct gap of 0.181 eV (GGA/HSE06), while a zero band gap was found at the LDA level of theory. Note that the use of pure GGA functional (NCP/PBE/1000 eV) provides similar results for the band gap (0.115 eV). There is a non-zero population at the Fermi level; thus, one can conclude that 2D polyguanidine behaves as a semimetal. The valence band maximum and conducting band minimum occur at the Γ-point. Moreover, valence band (VB) consists almost totally from 1s states of hydrogen. Thus, in contrast to graphene, which has no the intrinsic gap, 2D polyguanidine material can find useful applications in organic electronics and photonics.

3.2. Spectral characterisation and mechanical stability

To access information for spectral identification of 2D polyguanidine, we have calculated optical properties, namely, reflectivity, refractive index, conductivity and the loss function. Together with the absorption coefficient (α), these quantities are derivatives of the complex dielectric function $\varepsilon(\omega) = \varepsilon_1(\omega) + i\varepsilon_2(\omega)$ [47]. Thus, the absorption coefficient can be expressed as the following (Equation (2)) [47]:

$$\alpha(\omega) = \sqrt{2}\left[\sqrt{\varepsilon_1^2(\omega) + \varepsilon_2^2(\omega)} - \varepsilon_1(\omega)\right]^{1/2} \quad (2)$$

Equations for the rest of the optical properties along with the corresponding plots are presented in Figure S3 in the Supporting Information.

We have performed calculations of the optical properties for three directions of the polarised incident light, but due to the symmetry constraints, the directions [1 0 0] and [0 1 0] are identical. The obtained spectral results for the absorption coefficient α are illustrated in Figure 3.
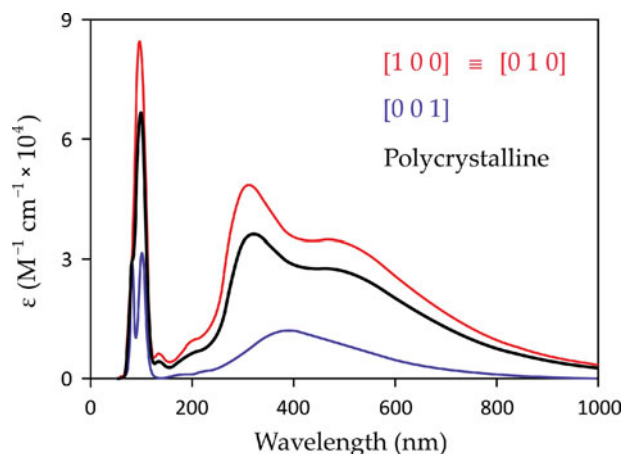

Figure 3. The calculated absorption spectrum of the 2D polyguanidine in three directions of the polarised incident light.

The direction [0 0 1] is the most important since it is perpendicular to the layer plane. As one can see in Figure 3, the results are in good agreement with the band structure calculations. The absorption covers entire visible region as well as the near infrared region. The lowest in energy transitions correspond to the directions [1 0 0] ≡ [0 1 0], while for the polarisation direction [0 0 1], the significant absorption starts in the visible region. Thus, one can expect that the 2D polyguanidine material represents the black matter. A strong absorption peak also occurs in the far UV region at about 100 nm.

Assignment of eight of the lowest in energy electronic transitions in the absorption spectrum of 2D polyguanidine is presented in Table 1, and the VB and conduction band (CB) are illustrated in Figure 4. As it follows from Table 1, electron transitions with maximum overlap occur from the VB in all the cases. The first intense absorption band with λ_{max} at about 480 nm (Figure 3) corresponds to a series of close-lying transitions from VB to the series of σ-bands (see Figure S4 in the Supporting Information). Meanwhile, the first electron transition occurs from the n-type VB to the π-type CB and has zero intensity because it is forbidden by symmetry.

Further, we have calculated the NMR parameters with the gauge-including projector augmented-wave method [48] and electric field gradient (EFG) values. The calculated data are listed in Table 2. Since the choice of NMR reference in theoretical calculations may become critical [49], we have discussed only the absolute values of magnetic shielding tensor (σ_{iso}). The values of σ_{iso} at the nitrogen atoms are equal to −35.35 ppm. This value much differs from that of molecular nitrogen −91.33 ppm [1] suggesting a denser electron arrangement around the nitrogen nuclei compared to molecular nitrogen. On the other hand, this value is lower than that of recently calculated carbon nitride phases (119–136 ppm) [50].
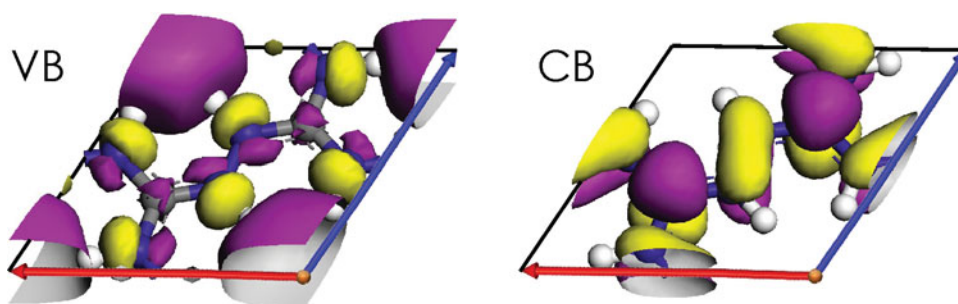
Figure 4. Valence and conduction bands of 2D polyguanidine.

Table 1. Energies (eV) and orbital assignment of the electron transitions in absorption spectrum of 2D polyguanidine.

State	E (eV)	Assignment	Overlap
S_1	0.100	VB→CB	0.997349
		VB→CB+4	0.001405
S_2	1.129	VB→CB+1	0.777131
		VB→CB+6	0.017527
S_3	2.427	VB→CB	0.001043
		VB→CB+4	0.899799
		VB→CB+9	0.085043
S_4	2.602	VB-2→CB+1	0.152486
		VB-1→CB+1	0.048119
		VB→CB+2	0.57177
		VB→CB+3	0.121563
		VB→CB+7	0.091096
S_5	2.602	VB-2→CB	0.047840
		VB-1→CB+2	0.151833
		VB→CB+2	0.121718
		VB→CB+3	0.577530
		VB→CB+8	0.091490
S_6	2.874	VB→CB+1	0.039989
		VB→CB+5	0.116447
		VB→CB+6	0.825739
S_7	3.027	VB→CB+1	0.005687
		VB→CB+5	0.880071
		VB→CB+6	0.108933
S_8	3.098	VB-4→CB+5	0.001178
		VB-2→CB+1	0.433164
		VB-2→CB+4	0.001515
		VB-1→CB	0.074667
		VB→CB+2	0.015658
		VB→CB+3	0.001502
		VB→CB+7	0.451683
		VB→CB+8	0.017764

Table 2. Chemical shielding and electric field gradient (EFG) tensors at the symmetry unique atoms in 2D polyguanidine.

	Shielding tensor			EFG tensor	
Atom	σ_{iso}[a] (ppm)	Δ[b] (ppm)	η[c]	C_Q[d] (MHz)	η_Q[e]
C	− 123.66	− 303.95	0.05	− 0.1312	0.00
N	− 35.35	− 414.82	0.33	− 5.9120	0.71
H	− 130.91	− 419.05	0.05	0.1376	0.47

[a] $\sigma_{iso} = (\sigma_{xx} + \sigma_{yy} + \sigma_{zz})/3$.
[b] $\Delta = \sigma_{zz} - \sigma_{iso}$.
[c] $\eta = (\sigma_{xx} - \sigma_{yy})/\Delta$.
[d] $C_Q = eQV_{zz}/h$, where V_{zz} is the largest component of the diagonalised EFG tensor, Q is the nuclear quadrupole moment, h is Plank's constant.
[e] $\eta Q = (V_{xx} - V_{yy})/V_{zz}$.

Table 3. Young modulus (E, GPa) and Poisson ratios (ν) for the studied 2D polyguanidine.

Axis	E (GPa)	Poisson ratios (ν)			
x	62.1692	E_{xy}	0.1696	E_{xz}	− 0.1468
y	62.1692	E_{yx}	0.1696	E_{yz}	− 0.1468
z	6.1762	E_{zx}	− 0.0146	E_{zy}	− 0.0146

In order to estimate mechanical stability of 2D polyguanidine, we have calculated elastic stiffness (C_{ij}) and compliance (S_{ij}) constants. The calculated values are gathered in Tables S2 and S3 in the Supporting Information. To be mechanically stable, a solid should satisfy the corresponding Born–Huang criteria. For the hexagonal lattice of the Laue class $6/m$ one can write six independent elastic constants [51]. But taking into account the known Cauchy relation $C_{66} = (C_{11} - C_{12})/2$ the number of independent constants is reduced to five. Thus, the studied system has the following four necessary and sufficient conditions for elastic stability (Equation (3)) [51]:

$$\begin{cases} C_{11} > |C_{12}| \, ; \, 2C_{13}^2 < C_{33}\,(C_{11} + C_{12}) \, ; \\ C_{44} > 0; \, 1/2\,(C_{11} - C_{12}) > 0. \end{cases} \quad (3)$$

Remarkably, all the independent elastic constants of 2D polyguanidine conform the Born–Huang criteria (Equation (3)) suggesting mechanical robustness of the studied material. Summary of the elastic properties, which include the Young's moduli and Poisson ratios are listed in Table 3. At the LDA level of theory, the mechanical stability is also confirmed.

3.3. Electron transport properties and QTAIM analysis

The density functional based tight binding method has been applied to calculate electron transport properties of the polyguanidine ribbon using the Slater–Koster library 'mio' [52]. We have built the ribbon of 26.6 Å wide
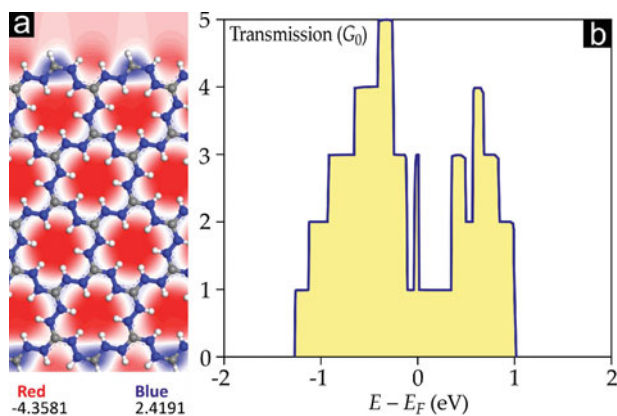
Figure 5. Plot of the electron potential field (a) and transmission function (b) of the transport device built using the polyguanidine ribbon.

Table 4. QTAIM properties (in a.u.) and the NICS values in the studied 2D polyguanidine.

CP	$\rho(\mathbf{r})$	$\nabla^2\rho(\mathbf{r})$	$h_e(\mathbf{r})$	NICS(0)	NICS(1)
RCP1	0.01180	0.06869	0.00377	-46.00	-34.24
RCP2	0.00963	0.00275	0.00043	-41.83	-34.34
BCP	0.02062	0.02676	-0.00278	–	–

and 44.8 Å long (Figure 5(a)). The obtained transmission spectrum is illustrated in Figure 5(b). Similar to the graphene ribbon with zigzag chains, the studied polyguanidine ribbon has a characteristic peak at the Fermi level (Figure 5(b)). It divides the transmission gap, which is rather narrow and equals to 0.46 eV.

It is known that the eigenstates of molecular projected self-consistent Hamiltonian are related to the poles of the Green's function [53]. Thus, the peaks in both the negative and positive energy regions of the transmission spectrum can be rationalised using molecular orbital information. This should be done in further more detailed studies.

The complete search of critical points (CPs), which are illustrated in Figure 1, has revealed the existence of H …H bonding interactions (see BCPs) and two ring critical points: formed partially (RCP1) or completely (RCP2) by the H …H bonds. The calculated QTAIM-parameters including electron density $\rho(\mathbf{r})$, its Laplacian $\nabla^2\rho(\mathbf{r})$ and Hamiltonian kinetic energy density $h_e(\mathbf{r})$ are listed in Table 4. These three quantities can be used to determine the peculiar nature of chemical bonds in this new 2D material. If $\rho(\mathbf{r})$ is about 0.1 a.u. and $\nabla^2\rho(\mathbf{r}) < 0$, then the bond is strong and formally covalent. In contrast, if $\rho(\mathbf{r})$ is about 0.01 a.u. and $\nabla^2\rho(\mathbf{r})$ is positive, then the bond corresponds to a closed-shell interaction (ionic, coordination) [54]. To distinguish the latter two bond types, one should analyse the $h_e(\mathbf{r})$ quantity. The negative $h_e(\mathbf{r})$

value specifies the coordination bond type and the positive one corresponds to the ionic bond [54]. Thus, as it follows from Table 4, the H …H interactions correspond to coordination bonds. Using the well-known Espinosa formula $E = 1/2v(\mathbf{r})$ [55], where $v(\mathbf{r})$ is the potential energy density obtained using the Abramov gradient expansion (Equation (4)) [56], the H …H bonding energy is equal to 22.2 kJ mol^{-1}.

$$v(\mathbf{r}) = -\frac{3}{5}(3\pi^2)^{2/3}\rho(\mathbf{r})^{5/3} - \frac{1}{12}\nabla^2\rho(\mathbf{r}) \qquad (4)$$

We should stress that the obtained H …H bonding energy is rather high compared to the average calculated energies of intra- and inter-molecular H …H bonding, which are about 11–13 kJ mol^{-1} [57–59]. The complete list of CPs is presented in Table S4 in the Supporting Information.

Finally, we have studied aromaticity of the rings formed upon guanidine polymerisation; the model compound used in this calculation is illustrated in Figure S5 in the Supporting Information. For this purpose, we have applied nucleus-independent chemical shift (NICS) values (Table 4). Remarkably, both the NICS(0) and NICS(1) values are strongly negative. This means the existence of diatropic currents and thus the aromatic character of the discussed rings. This phenomenon requires a more detailed analysis in further studies.

4. Conclusions

In summary, we have reported a comprehensive study of a new 2D material based on polyguanidine. The high-quality band structure calculations have revealed a quasi-metal character of this material with a tiny band gap (0.181 eV). Similar quasi-metal properties have been recently found in 2D biphenylene-based polymer [60]. Such a small band gap provides 2D polyguanidine interesting properties, which can be useful for applications in electronics and photonics. The studied polyguanidine sheet is dynamically and mechanically stable; however, the mechanical robustness is moderate, which is following from the Young modulus values. The phonon dispersion calculations reveal that the N–H bonds have a tendency to out-of-the plane alignment. Thus, it can result in the existence of a close-lying non-planar structure, which is expected to have a wider intrinsic gap; this is the issue of further studies.

Acknowledgments

PDC supercomputer use. The computations were performed on resources provided by the Swedish National Infrastructure for Computing (SNIC) at the Parallel Computer Center (PDC) through the project 'Multiphysics Modeling of Molecular Materials', SNIC 020/11-23.

Disclosure statement

No potential conflict of interest was reported by the authors.

Funding

ORCID

Sergey V. Bondarchuk http://orcid.org/0000-0002-3545-0736

References

[1] S.V. Bondarchuk and B.F. Minaev, Comput. Mater. Sci. **133**, 122 (2017).
[2] J. Lee, W.-C. Tian, W.-L. Wang, and D.-X. Yao, Sci. Rep. **5**, 11512 (2015).
[3] H. Shioyama, J. Mater. Sci. Lett. **20**, 499 (2001).
[4] P. Avouris and F. Xia, MRS Bull. **37**, 1225 (2012).
[5] R. Mas-Ballesté, C. Gómez-Navarro, J. Gómez-Herrero, and F. Zamora, Nanoscale **3**, 20 (2011).
[6] K.S. Novoselov, A.K. Geim, S.V. Morozov, D. Jiang, Y. Zhang, S.V. Dubonos, I.V. Grigorieva, and A.A. Firsov, Science **306**, 666 (2004).
[7] A.H. Castro Neto, F. Guinea, N.M.R. Peres, K.S. Novoselov, and A.K. Geim, Rev. Mod. Phys. **81**, 109 (2009).
[8] T.M. Klapötke, Struct. Bond. **125**, 85 (2007).
[9] T.M. Klapötke, M.Q. Kurz, R. Scharf, P.C. Schmid, J. Stierstorfer, and M. Sućeska, ChemPlusChem **79**, 1 (2014).
[10] L. He, G.-H. Tao, D.A. Parrish, and J.M. Shreeve, Chem. Commun. **49**, 10329 (2013).
[11] R. Wang, Y. Guo, Z. Zeng, and J.M. Shreeve, Chem. Commun. 2697 (2009).
[12] M. Göbel and T.M. Klapötke, Z. Anorg. Allg. Chem. **633**, 1006 (2007).
[13] H. Gao, Y.-H. Joo, D.A. Parrish, T. Vo, and J.M. Shreeve, Chem. Eur. J. **17**, 4613 (2011).
[14] D.E. Chavez, B.C. Tappan, B. Aaron Mason, and D. Parrish, Prop. Explos. Pyrotech. **34**, 475 (2009).
[15] A. Hammer, M.A. Hiskey, G. Holl, T.M. Klapötke, K. Polborn, J. Stierstorfer, and J.J. Weigand, Chem. Mater. **17**, 3784 (2005).
[16] C. Zheng, Y. Chu, L. Xu, W. Lei, F. Wang, and M. Xia, J. Mol. Model. **23**, 12 (2017).
[17] R. Wang, Y. Guo, R. Sa, and J.M. Shreeve, Chem. Eur. J. **16**, 8522 (2010).
[18] R. Custelcean, N.J. Williams, and C.A. Seipp, Angew. Chem. **127**, 10671 (2015).
[19] A. Pantos, I. Tsogas, and C.M. Paleos, Biochim. Biophys. Acta **1778**, 811 (2008).
[20] P. Andrew Evans and T. Manangan, Tetrahedron Lett. **42**, 6637 (2001).
[21] C. Liu, Q. Deng, G. Fang, X. Huang, S. Wang, and J. He, ACS Appl. Mater. Interfaces **7**, 20430 (2015).
[22] Y. Gu, Y. Guo, K. Sun, R. Su, Q. Deng, H. Li, and S. Wang, RSC Adv. **6**, 41707 (2016).
[23] X.A. Jeanbourquin, X. Li, C. Law, P.R.F. Barnes, R. Humphry-Baker, P. Lund, M.I. Asghar, and B.C. O'Regan, J. Am. Chem. Soc. **136**, 7286 (2014).
[24] N. De Marco, H. Zhou, Q. Chen, P. Sun, Z. Liu, L. Meng, E.-P. Yao, Y. Liu, A. Schiffer, and Y. Yang, Nano Lett. **16**, 1009 (2016).
[25] M.A. Yarmolenko, A.A. Rogachev, V.E. Agabekov, A.V. Rogachev, V.A. Dobysh, V.A. Tarasevich, and D.V. Tapal'skii, Russ. J. Appl. Chem. **85**, 678 (2012).
[26] B. Dietrich, D.L. Fyles, T.M. Fyles, and J.-M. Lehn, Helv. Chim. Acta **62**, 2763 (1979).
[27] S.J. Clark, M.D. Segall, C.J. Pickard, P.J. Hasnip, M.J. Probert, K. Refson, and M.C. Payne, Z. Kristallogr. **220**, 567 (2005).
[28] Materials Studio 7.0 (Accelrys, Inc., San Diego, CA, 2013).
[29] J.P. Perdew, K. Burke, and M. Ernzerhof, Phys. Rev. Lett. **77**, 3865 (1996).
[30] J.P. Perdew, A. Ruzsinszky, G.I. Csonka, O.A. Vydrov, G.E. Scuseria, L.A. Constantin, X. Zhou, and K. Burke, Phys. Rev. Lett. **100**, 136406 (2008).
[31] J. Heyd and G. Scuseria, J. Chem. Phys. **121**, 1187 (2004).
[32] G.M. Dongho Nguimdo and D.P. Joubert, Eur. Phys. J. B **88**, 113 (2015).
[33] A. Tkatchenko and M. Scheffler, Phys. Rev. Lett. **102**, 073005 (2009).
[34] D.M. Ceperley and B.J. Alder, Phys. Rev. Lett. **45**, 566 (1980).
[35] J.P. Perdew and A. Zunger, Phys. Rev. B **23**, 5048 (1981).
[36] F. Ortmann, F. Bechstedt, and W.G. Schmidt, Phys. Rev. B **73**, 205101 (2006).
[37] J.A. Alarco, A. Chou, P.C. Talbota, and I.D.R. Mackinnon, Phys. Chem. Chem. Phys. **16**, 24443 (2014).
[38] S.V. Bondarchuk and B.F. Minaev, RSC Adv. **5**, 11558 (2015).
[39] G. Kresse and D. Joubert, Phys. Rev. B **59**, 1758 (1999).
[40] P. Giannozzi, S. Baroni, N. Bonini, M. Calandra, R. Car, C. Cavazzoni, D. Ceresoli, G.L. Chiarotti, M. Cococcioni, I. Dabo, A. Dal Corso, S. Fabris, G. Fratesi, S. de Gironcoli, R. Gebauer, U. Gerstmann, C. Gougoussis, A. Kokalj, M. Lazzeri, L. Martin-Samos, N. Marzari, F. Mauri, R. Mazzarello, S. Paolini, A. Pasquarello, L. Paulatto, C. Sbraccia, S. Scandolo, G. Sclauzero, A.P. Seitsonen, A. Smogunov, P. Umari, and R.M. Wentzcovitch, J. Phys.: Condens. Matter **21**, 395502 (2009).
[41] A. Otero-De-La-Roza, E.R. Johnson, and V. Luaña, Comput. Phys. Commun. **185**, 1007 (2014).
[42] S.V. Bondarchuk and B.F. Minaev, Phys. Chem. Chem. Phys. **19**, 6698 (2017).
[43] M.J. Frisch, G.W. Trucks, H.B. Schlegel, G.E. Scuseria, M.A. Robb, J.R. Cheeseman, G. Scalmani, V. Barone, B. Mennucci, G.A. Petersson, H. Nakatsuji, M. Caricato, X. Li, H.P. Hratchian, A.F. Izmaylov, J. Bloino, G. Zheng, J.L. Sonnenberg, M. Hada, M. Ehara, K. Toyota, R. Fukuda, J. Hasegawa, M. Ishida, T. Nakajima, Y. Honda, O. Kitao, H. Nakai, T. Vreven, J.A. Montgomery Jr., J.E. Peralta,

F. Ogliaro, M.J. Bearpark, J. Heyd, E.N. Brothers, K.N. Kudin, V.N. Staroverov, R. Kobayashi, J. Normand, K. Raghavachari, A.P. Rendell, J.C. Burant, S.S. Iyengar, J. Tomasi, M. Cossi, N. Rega, N.J. Millam, M. Klene, J.E. Knox, J.B. Cross, V. Bakken, C. Adamo, J. Jaramillo, R. Gomperts, R.E. Stratmann, O. Yazyev, A.J. Austin, R. Cammi, C. Pomelli, J.W. Ochterski, R.L. Martin, K. Morokuma, V.G. Zakrzewski, G.A. Voth, P. Salvador, J.J. Dannenberg, S. Dapprich, A.D. Daniels, O. Farkas, J.B. Foresman, J.V. Ortiz, J. Cioslowski, and D.J. Fox, *Gaussian 09, Revision A.02* (Gaussian, Inc., Wallingford, CT, 2009).

[44] A.D. Becke, J. Chem. Phys. **98**, 5648 (1993).

[45] R. Krishnan, J.S. Binkley, R. Seeger, and J.A. Pople, J. Chem. Phys. **72**, 650 (1980).

[46] W. Setyawan and S. Curtarolo, Comput. Mater. Sci. **49**, 299 (2010).

[47] M. Sheik-Bahae, *Nonlinear Optics Basics. Kramers-Kronig Relations in Nonlinear Optics* (Academic Press, Amsterdam, 2005).

[48] C.J. Pickard and F. Mauri, Phys. Rev. B **63**, 245101 (2001).

[49] M. Dračínský, M. Šála, B. Klepetářová, J. Šebera, J. Fukal, V. Holečková, Y. Tanaka, R. Nencka, and V. Sychrovský, J. Phys. Chem. B **120**, 915 (2016).

[50] S.V. Bondarchuk and B.F. Minaev, Submitted to Journal (2017).

[51] F. Mouhat and F.-X. Coudert, Phys. Rev. B **90**, 224104 (2014).

[52] M. Elstner, D. Porezag, G. Jungnickel, J. Elsner, M. Haugk, Th. Frauenheim, S. Suhai, and G. Seifert, Phys. Rev. B **58**, 7260 (1998).

[53] Z.Y. Li and D.S. Kosov, J. Phys. Chem. B **110**, 9893 (2006).

[54] R.F.W. Bader, *Atoms in Molecules: A Quantum Theory* (Oxford University Press, New York, 1990).

[55] E. Espinosa, E. Molins, and C. Lecomte, Chem. Phys. Lett. **825**, 170 (1998).

[56] Yu.A. Abramov, Acta Cryst. **A53**, 264 (1997).

[57] S.V. Bondarchuk, B.F. Minaev, and A.Yu. Fesak, Int. J. Quantum Chem. **113**, 2580 (2013).

[58] S. Scheiner, Int. J. Quantum Chem. **110**, 2775 (2010).

[59] M.V. Vener, A.N. Egorova, D.P. Fomin, and V.G. Tsirelson, J. Phys. Org. Chem. **22**, 177 (2009).

[60] N.N. Karaush, S.V. Bondarchuk, G.V. Baryshnikov, V.A. Minaeva, W.-H. Sun, and B.F. Minaev, RSC Adv. **6**, 49505 (2016).